Programmable Optical Pulse Burst Manipulation Using a Virtually Imaged Phased Array (VIPA) Based Fourier Transform Pulse Shaper

Ghang-Ho Lee, *Student Member, IEEE*, and Andrew M. Weiner, *Fellow, IEEE*

***Abstract*—This paper presents the first application of the virtually imaged phased array (VIPA) in a Fourier transform pulse shaper for programmable manipulation of optical pulse bursts using a spatial light modulator (SLM). Due to the periodicity of the VIPA spectral dispersion function, a periodic spectral phase function is automatically generated from a single-period spatial phase function. Experimental results and theoretical simulations were compared with quadratic, cubic, and m-sequence mask patterns. The data demonstrate programmable manipulations of the pulse envelopes, in good agreement with the theory.**

***Index Terms*—Optical pulse generation, optical pulse shaping, spatial disperser, ultrafast optics.**

I. Introduction

PULSE shaping, which allows manipulation of femtosecond optical pulses according to user needs, is now a well-established technique. The most widely adopted pulse shaping method, Fourier transform pulse shaping, uses a pair of diffraction gratings as spatial dispersers, a pair of Fourier transform lenses to separate the optical spectrum, and a spatial mask or modulator array to manipulate spatially dispersed optical frequency components in parallel [1], [2]. This technique is now applied in fields ranging from optical communications to coherent control of quantum mechanical motions to optical pulse compression at the few-cycle level.

For applications in optical communications, for example, there is interest in extending pulse shaping to larger time apertures, which requires higher spectral resolution. This requires larger spectral dispersion compared to diffraction gratings. One possibility that has been reported involves using modified arrayed waveguide grating (AWG) structures. Some of the early papers [3], [4] discussed how AWGs could support larger time apertures. Another possibility, which is presented in this paper, is to use the virtually imaged phased array (VIPA) as the spatial disperser. The VIPA may be considered as a side-entrance etalon device that achieves angular dispersion through multiple beam interference. The VIPA has advantages compared to conventional dispersers like diffraction gratings, such as polarization insensitivity, compactness, larger angular dispersion, potential for finer spectral resolutions, and potentially low cost [5], [6].

Here, for the first time in the authors' knowledge, a programmable Fourier transform pulse shaping using a VIPA-based pulse shaper is demonstrated. Another important aspect of this work relates to the periodic spectral dispersion behavior of the VIPA, which has free spectral range (FSR) equal to the inverse of the round trip time within the VIPA etalon. This behavior enables to apply a periodic spectral phase function by using only a single-period spatial phase function at the Fourier plane, resulting in the generation of programmable pulse bursts whose envelopes are controlled via the pulse shaper settings.

Previously, the VIPA has been applied in a pulse shaping geometry for dispersion compensation in fiber optic wavelength division multiplexing (WDM) systems [7]–[9]. These studies used dispersion compensating fiber (DCF) to compensate low-order dispersion and the VIPA Fourier transform pulse shaper to compensate residual high-order dispersion within the fiber links. The pulse shaper in these experiments was composed of a VIPA as spatial disperser with a curved mirror placed at the Fourier plane. However, the authors of these studies analyze their results in terms of ray tracing and path length differences and do not point out that the set up can be understood simply as a Fourier transform pulse shaper that imposes a spatial phase function at the Fourier planes. A VIPA-based direct space-to-time pulse shaper has been used for radio frequency arbitrary waveform generation [10]. Recently, VIPA-based Fourier transform pulse shapers have been used as optical encoders/decoders in optical code division multiple access (OCDMA) systems [11]. Here, the VIPA Fourier transform pulse shaper is used to produce desired optical code sequences that are unique for each user in an optical network. This system also uses the VIPA Fourier transform pulse shaper in reflective geometry by placing a fixed mask and a turn-around mirror at the Fourier plane. The phase mask applies a binary code, i.e., either zero or π phase shift, to different spatially dispersed wavelength components. By replacing the fixed mask (shaped mirror) with a programmable mask, i.e., a liquid crystal phase spatial light modulator (SLM), more flexible pulse shaping including dispersion compensation and optical encoding/decoding should be possible. Here, the authors demonstrate, for the first time in their knowledge, such programmable pulse shaping using a VIPA-based Fourier transform pulse shaper.

The remainder of this paper is structured as follows. Section II explains new concepts in this work relating to the

Manuscript received January 9, 2005; revised June 10, 2005.

The authors are with the School of Electrical and Computer Engineering, Purdue University, West Lafayette, IN 47906-1285 USA (e-mail: leeg@purdue.edu; amw@ecn.purdue.edu).

Digital Object Identifier 10.1109/JLT.2005.857739

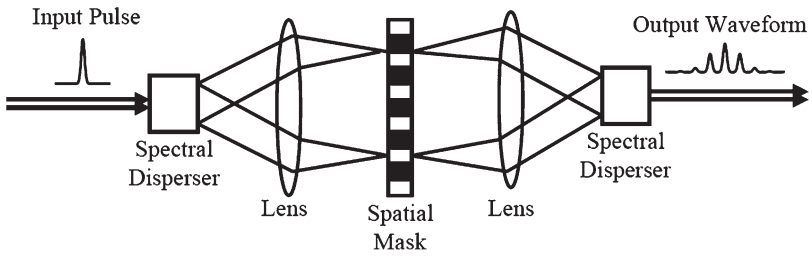

Fig. 1. Generic layout of the Fourier transform pulse shaper.

generation of periodic phase functions and consequently to optical pulse burst generation. Section III discusses the experimental setup and apparatus design in detail. Section IV presents a number of examples of pulse shaping results, and the conclusion is in Section V.

II. Pulse Shaping and Optical Pulse Burst Generation

Fig. 1 shows the generic layout of a Fourier transform pulse shaper [1], [2]. It consists of a pair of spatial dispersers, a pair of lenses in 4*f* configuration, and a spatial mask. The frequency (wavelength) components within the incident pulse are angularly dispersed by the first spectral disperser and then focused to small diffraction-limited spots at the Fourier plane, where the frequency components are spatially separated along one dimension. Essentially, the first focal lens performs a spatial Fourier transform, which converts the angular dispersion from the disperser to a spatial separation at the Fourier plane. A spatial mask or an SLM is placed in this plane to manipulate the spatially dispersed optical frequency components. After manipulation by the spatial mask, the second lens and spatial disperser pair recombine all the frequency components into a single collimated beam. The resulting output pulse shape is determined by the Fourier transform of the spatial mask pattern.

The spectrum of the pulse emerging from the Fourier transform pulse shaper can be written as

$$E_{\rm out}(\omega) = E_{\rm in}(\omega) \times H(\omega) \tag{1}$$

where $E_{\rm out}(\omega)$ and $E_{\rm in}(\omega)$ are the complex spectral amplitudes of the output and input fields, respectively, and $H(\omega)$ is the frequency response function of the filter synthesized via the pulse shaper. For a pulse shaper with a grating as the spectral disperser, the applied filter transfer function is related to the spatial mask function by [2]

$$H(\omega) = \int M(x) \exp\left(\frac{-2(x-\alpha\omega)^2}{w_0^2}\right) {\rm d}x \tag{2}$$

where $M(x)$ is the spatial mask function as a function of spatial position x, α denotes the spatial dispersion, and w_0 denotes the beam radius of individual frequency components at the Fourier plane. In this paper, we will specialize to the case of phase-only masks, where the spatial mask function can be expressed as

$$M(x) \sim \exp\left(-i\Phi(x)\right). \tag{3}$$

Note that the convolution in (2) represents a smearing of the spectral filter function compared to the spatial mask due to the finite size of individual frequency components at the Fourier plane. We neglect this smearing in most of this paper. Note also that we do not explicitly consider any space–time coupling effects that arise due to diffraction from features in the spatial mask [12]. In our experiments, any spatial variation in the shaped pulse is eliminated by coupling into single-mode fiber; equation (2) fully accounts for the spectral filter that results when the space–time field from the shaper is coupled into the fiber [2]. The resulting shaped pulse in time domain can be obtained by performing the Fourier transform on (1) and is given by

$$e_{\rm out}(t) = e_{\rm in}(t) * h(t) \tag{4}$$

where $e_{\rm out}(t)$, $e_{\rm in}(t)$, and $h(t)$ are the inverse Fourier transform of $E_{\rm out}(\omega)$, $E_{\rm in}(\omega)$, and $H(\omega)$, respectively.

For the conventional grating-based Fourier transform pulse shaper, the spectral filter function $H(\omega)$ is essentially a scaled version of the spatial mask function $M(x)$ as illustrated in (2). However, for the VIPA-based Fourier transform pulse shaper, in which VIPA replaces the grating as spectral disperser, new behavior arises due to the properties of the VIPA, namely, periodic spectral dispersion. The VIPA is a modified version of the Fabry–Pérot etalon composed by two glass plates, namely, incident glass plate and transmission glass plate, with a different reflectivity coating. The incident glass plate has a nearly 100% total reflectivity, except for a small window that is an anti-reflection coated for optical beam input. The transmission glass plate typically has 95–99% partial reflectivity to transmit a small portion of the optical beam out of etalon cavity and reflect the rest of the beam back. Due to the high reflectivity on both sides of glass plates, the injected optical beam experiences multiple reflections within the etalon cavity, thus producing multiple diverging beams through the transmission glass plate. Diverging beams interfere with each other as they propagate, separating different wavelength components in the beam with respect to the output angle. As a result, the VIPA acts as spatial disperser, which separates different wavelength components within the input optical beam at different locations.

Fig. 2 illustrates schematically the relationship between the realized spectral phase function $\Psi(\omega)$ and the spatial phase function $\Phi(x)$ for the VIPA Fourier transform pulse shaper. Fig. 2(a) shows an example of the VIPA response (angular dispersion) with frequency ω as a function of the spatial position x at the Fourier plane. The key point is that the VIPA exhibits many closely spaced diffraction orders. The phase shift $\Phi(x_0)$

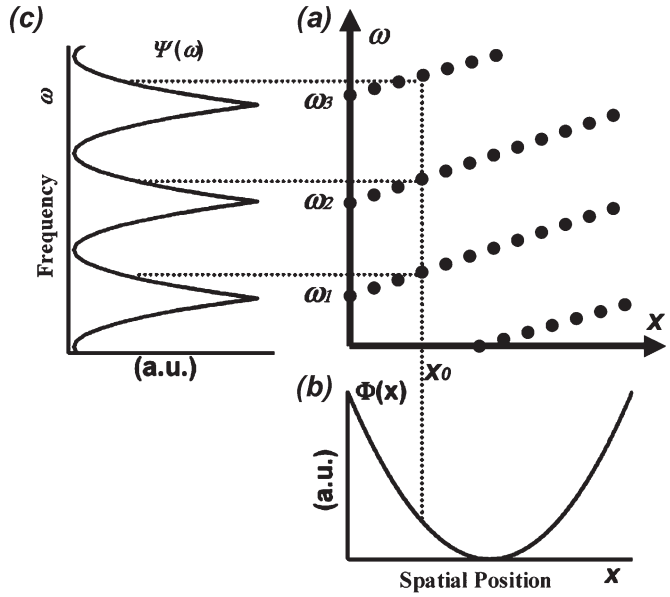

Fig. 2. VIPA Fourier transform pulse shaper response. (a) Example of VIPA response (angular dispersion) with frequency ω as a function of spatial position x. (b) Example of single-period quadratic spatial phase function $\Phi(x)$ applied at Fourier plane by spatial mask. (c) Resulting periodic quadratic spectral phase function $\Psi(\omega)$ applied to the input spectrum.

imparted by the spatial mask at spatial position x_0 in the Fourier plane determines the phases at frequencies ω_1, ω_2, and ω_3 in the spectral plane, i.e., $\Psi(\omega_1) = \Psi(\omega_2) = \Psi(\omega_3) = \Phi(x_0)$. Fig. 2(b) shows an example of a single-period quadratic spatial phase function $\Phi(x)$ applied at the Fourier plane by a spatial mask. Fig. 2(c) shows the resulting periodic quadratic spectral phase function $\Psi(\omega)$ applied to the input spectrum.

The imposition of a periodic spectral phase function onto a short pulse is known to result in the generation of a burst of optical pulses [13]. Approximating the VIPA spectral dispersion within a single diffraction order as linear, we can write (1) as

$$\begin{aligned} E_{\text{out}}(\omega) &= E_{\text{in}}(\omega)H(\omega) \\ &= E_{\text{in}}(\omega)\left[\sum_k S(\omega - k\Delta\omega)\right] \\ &= E_{\text{in}}(\omega)\left[S(\omega) * \sum_k \delta(\omega - k\Delta\omega)\right] \end{aligned} \tag{5}$$

where $H(\omega)$ is now a periodic function with period $\Delta\omega$ equal to the VIPA FSR. $S(\omega)$ is the effective filter function for a single FSR in frequency, which is directly related to the spatial phase function $\Phi(x)$ via

$$S(\omega) \sim A(\omega)\exp\left(-i\Phi(\alpha x)\right) \tag{6}$$

where $A(\omega)$ is the VIPA pulse shaper amplitude transmission spectrum for a single FSR. Here, in addition to linear spectral dispersion, we have assumed that the convolution in (2) can be ignored; this is valid when the spatial masking function varies slowly with respect to the spot size of an individual frequency component at the Fourier plane. Effects arising when this assumption is not satisfied are discussed in [2]; details concerning the VIPA spectral dispersion and focused field distribution are presented in [6]. The temporal output is obtained by performing the inverse Fourier transform of (5), which yields

$$e_{\text{out}}(t) \sim e_{\text{in}}(t) * \left[s(t)\sum_l \delta\left(t - l\frac{2\pi}{\Delta\omega}\right)\right] \tag{7}$$

where $e_{\text{out}}(t)$, $e_{\text{in}}(t)$, and $s(t)$ are the inverse Fourier transform of $E_{\text{out}}(\omega)$, $E_{\text{in}}(\omega)$, and $S(\omega)$, respectively. The temporal output $e_{\text{out}}(t)$ is proportional to the temporal input $e_{\text{in}}(t)$ convolved with a set of delta functions spaced by the inverse of the FSR $(2\pi/\Delta\omega)$. For an input pulse shorter than $2\pi/\Delta\omega$, this results in a burst of periodically spaced output pulses. The amplitudes of the individual pulses are determined by the envelope function $s(t)$, the inverse Fourier transform of the single-period spectral filter function $S(\omega)$.

A simulated example comparing the results of applying a single-period phase function and a periodic phase function is shown in Fig. 3. The input optical spectrum $E_{\text{in}}(\omega)$ is the same in all cases, and for this example we set $A(\omega) = 1$. Three different phase functions $\Psi(\omega)$ and resulting output intensity profiles $I_{\text{out}}(t)$ are shown as the middle and right traces, respectively. Fig. 3(a) shows the result when no phase is applied to the input spectrum ($\Psi_a(\omega) = 0$). The resultant output pulse $I_{a,\text{out}}(t)$ is a single narrow pulse centered at zero delay in the temporal window. Fig. 3(b) shows the result when a single-period quadratic phase function $\Psi_b(\omega)$ is applied to the input spectrum. The resultant output pulse $I_{b,\text{out}}(t)$ is broadened in the time domain and chirped compared to the result in Fig. 3(a). Fig. 3(c) shows the result when a periodic quadratic phase function $\Psi_c(\omega)$ is applied to the input spectrum. Instead of a single broadened pulse as in Fig. 3(b), a burst of identical pulses with different amplitudes is generated as shown in $I_{c,\text{out}}(t)$. For the VIPA Fourier transform pulse shaper, the periodic spectral phase function $\Psi(\omega)$, similar to the one shown in the middle trace in Fig. 3(c), can be generated automatically from a nonperiodic spatial phase function $\Phi(x)$ provided that the input bandwidth exceeds the VIPA FSR. This allows us to perform experiments in which we generate optical pulse bursts and manipulate the envelopes of their bursts via pulse shaper control.

III. Experimental Setup

Fig. 4 shows the schematic diagram of the experimental set up. The Fourier transform pulse shaper in Fig. 1 was modified to a reflective geometry for simplicity, due to symmetry in the geometrical configuration, by inserting a mirror at the Fourier plane after the SLM (spatial mask) and separating the input and the reflected output by a circulator. An erbium fiber ring laser producing 250-fs pulses with a repetition rate of 50 MHz centered at 1545 nm with 12-nm bandwidth was used as the source. By using a fiber collimator and a semicylindrical lens, the source is fed into the VIPA. The air-spaced VIPA, with an FSR of 400 GHz, spatially disperses the line-focused different frequency (wavelength) components of the source. The spatially dispersed frequency components are focused at the Fourier plane, where the SLM is located, by using 190-mm focal length lens. The SLM at the Fourier plane modulates the phases of individual wavelength components

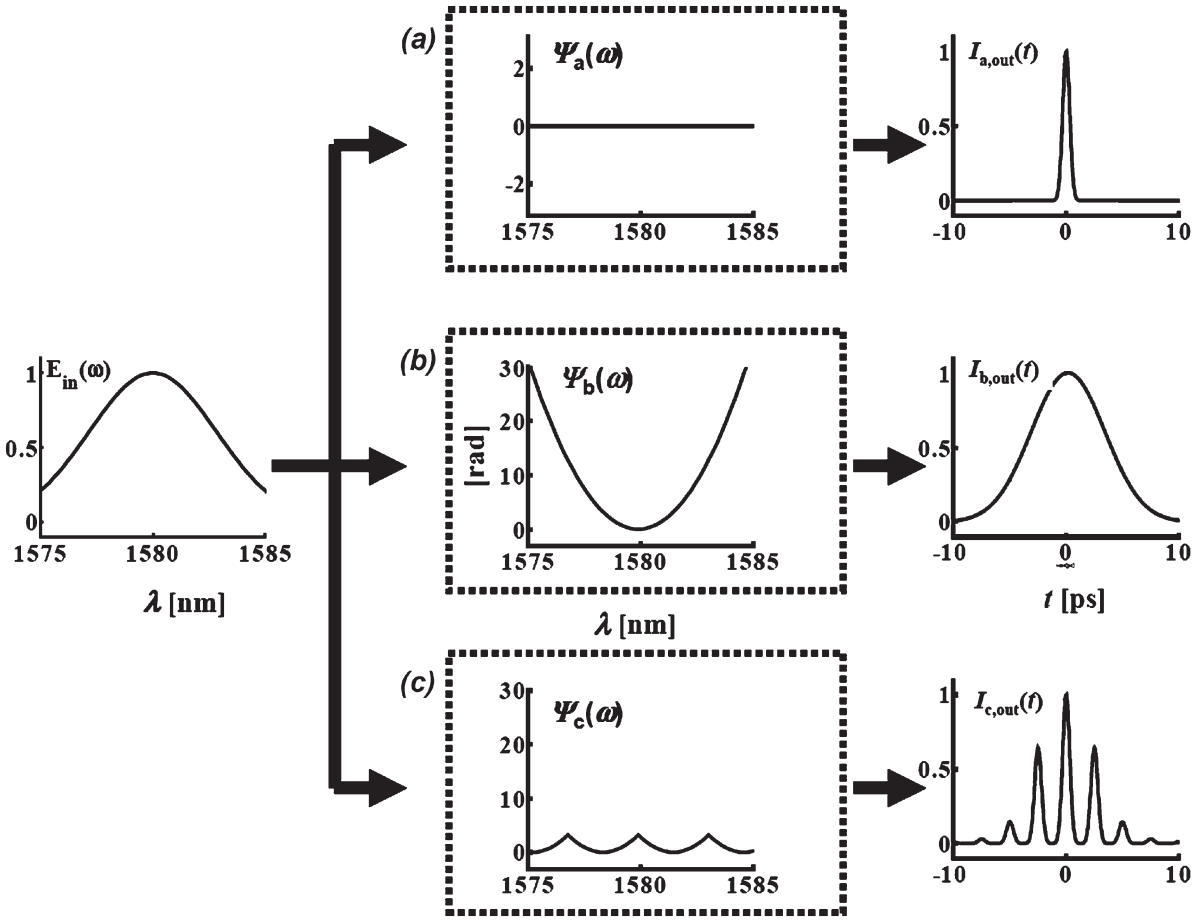

Fig. 3. Schematic diagram illustrating the effect of applying different spatial masks to identical inputs $E_{\rm in}(\omega)$. Input optical spectrum (left trace), applied phase functions (middle traces), resulting output intensity correlations (right traces), $I_{a,\rm out}(t)$, $I_{b,\rm out}(t)$, $I_{c,\rm out}(t)$. (a) No phase applied $\Psi_a(\omega)$. (b) Single-period quadratic phase function applied $\Psi_b(\omega)$. (c) Periodic quadratic phase function applied $\Psi_c(\omega)$.

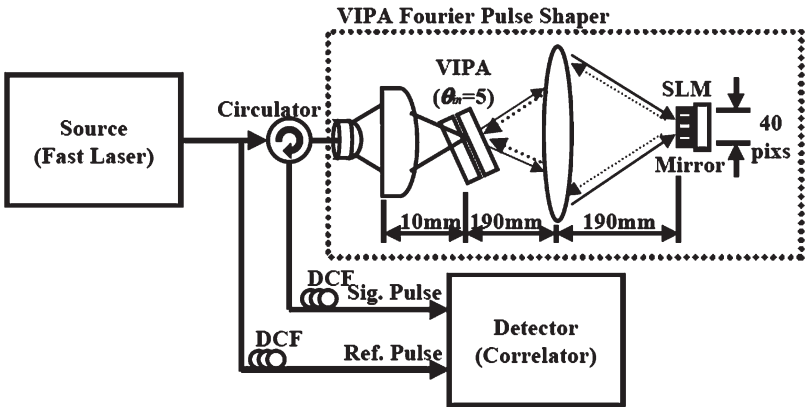

Fig. 4. Experimental apparatus for programmable Fourier transform pulse shaper based on VIPA.

according to desired phase function $\Phi(x)$. For the reflected path, the lens and the VIPA recombine the phase-modulated frequency components into a single output beam that is coupled back into the fiber.

Fig. 5 shows the power transmission function of the VIPA pulse shaper. The amplitude transmission for the $A(\omega)$ in (6) is obtained by taking the square root of this data over one FSR. This $A(\omega)$ factor is used in our simulations of the pulse shaping results shown later in Figs. 6 and 7. However, additional simulations (not shown) indicate that the effect of including the $A(\omega)$ factor is relatively small.

The SLM is a standard liquid crystal modulator array composed of 128 elements with dimensions of 2 mm $\times$ 100 μm per element and having roughly 3-μm gap between each element. The SLM was programmed to apply a desired phase function $\Phi(x)$ by a laboratory computer through a controller. We have applied both continuous gray level phase modulation and discrete binary level phase modulation to the SLM.

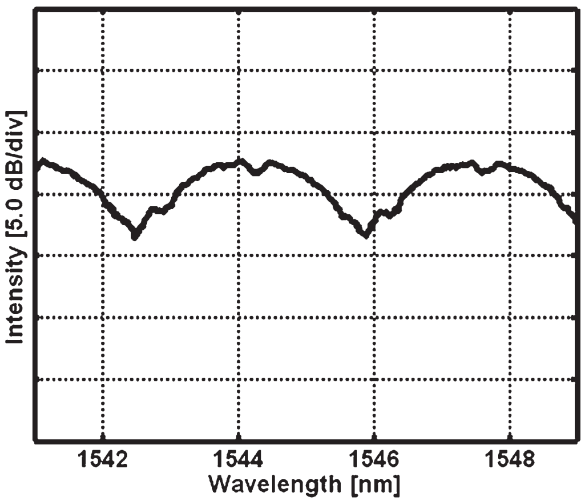

Fig. 5. Measured VIPA power transmission function.

Other design parameters used in the experimental setup include the focal length of semicylindrical lens ($\sim$ 10 mm) and the input angle into the VIPA ($\sim 5^{\circ}$). The total spatial spread of the incident spectrum on the SLM at the Fourier plane was 4.0 mm (corresponding to a VIPA FSR of 3.2 nm), which covers 40 SLM pixels. In most of our experiments, the SLM was programmed to provide quadratic and cubic phase functions $\Phi(x)$ by using 40 adjacent discrete pixels within the SLM. The spatial phase function programmed onto the SLM can be written as

$$\Phi(n) = \phi_{\text{quad}}\left(n - \frac{N_{\text{BW}}}{2} - N_{q,\text{shift}}\right)^2 + \phi_{\text{cubic}}\left(n - \frac{N_{\text{BW}}}{2} - N_{c,\text{shift}}\right)^3 \quad (8)$$

where $\Phi(n)$ is the phase at the nth pixel of the programmable SLM. It has the same meaning as $\Phi(x)$, but with spatial position x digitized to pixel number n. ϕ_{quad} and ϕ_{cubic} are the amplitudes of the quadratic and cubic phases involved in pulse shaping operation, N_{BW} (equal to 40) denotes the total number of pixels, and $N_{q,\text{shift}}$ and $N_{c,\text{shift}}$ denote shifts in the applied quadratic and cubic phase functions.

The output of the VIPA Fourier transform pulse shaper was connected via fiber to an intensity correlator using $\sim$ 250-fs reference pulses taken directly after the source input. DCF was used to balance the dispersion of the fiber used to relay the pulses to the cross correlator. To a good approximation, the cross-correlation measurement yields the intensity profiles of the shaped pulse bursts generated by the VIPA Fourier transform pulse shaper.

IV. Experimental Results

We have obtained a number of results in manipulation of optical pulse bursts via the periodic phase modulation imparted using the VIPA Fourier transform pulse shaper. Figs. 6–8 are examples. The top traces in these figures are the spectral phase functions $\Psi(\omega)$ that are applied to the input optical spectrum. The middle traces are the experimental cross-correlation measurements of the temporal intensity profiles obtained at the pulse shaper output. The bottom traces are the simulated results obtained by multiplying the input optical spectrum $E_{\text{in}}(\omega)$ with the periodic filter transfer function $H(\omega)$ and performing inverse Fourier transform. The dashed lines on the bottom traces are the simulated temporal envelope functions $|s(t)|^2$ of the optical pulse bursts that determine the relative intensities of the individual pulses in the generated bursts. $s(t)$ is obtained by performing the inverse Fourier transform of the single-period filter transfer function $S(\omega)$ in (5) and (6).

Fig. 6 shows results when a periodic quadratic phase function with a period of 400 GHz (equal to the VIPA FSR) is applied. The cubic phase term is set to zero ($\phi_{\text{cubic}} = 0$). The phase function repeats approximately four times within the total input optical bandwidth. For Fig. 6(a), the quadratic phase factor ϕ_{quad} is set to 0.005 and $N_{q,\text{shift}} = 0$. This results in a symmetric quadratic phase variation ranging between zero and $\pi/2$ within a single period. The resulting output contains three observable pulses consistent with the predicted envelope function shown in the dashed line in the bottom trace. Fig. 6(b) shows the case when the maximum phase variation is increased to $\pi(\Phi_{\max}(n) = \pi)$. The quadratic phase factor ϕ_{quad} was increased to 0.01 and the other parameters remained same as the case in Fig. 6(a). The resulting output is a burst of five distinct optical pulses. It is clear from Fig. 6(a) and (b) that increasing the magnitude of quadratic phase variation broadens the temporal window and increases the number of pulses in the burst. There is some deviation between experimental results (middle trace) and simulated result (bottom trace) of Fig. 6(b); in particular, the pulse at $t = 0$ is higher for the experiment than for the simulation. We attribute this to a small phase calibration error for the SLM, since a phase calibration error modifies the modulo-2π operation and intensity at $t = 0$ for the case of large total phase swing. Otherwise, the experimental and simulated results are in good agreement.

Fig. 6(c) and (d) shows cases where the phase functions are spectrally shifted. The spatial phase function within a single period in both cases is given by

$$\Phi(n) = \phi_{\text{quad}}\left(n - \frac{N_{\text{BW}}}{2} - N_{q,\text{shift}}\right)^2 \quad (9)$$

where all parameters are the same as the case in Fig. 6(b), except $N_{q,\text{shift}} \neq 0$. This yields asymmetric parabolas for the phase function as shown in the top traces of Fig. 6(c) and (d). In Fig. 6(c), the spectral phase function $\Psi(\omega)$ is spectrally shifted by 300 GHz (2.4 nm), which corresponds to 3/4 of a single period (VIPA FSR): $N_{q,\text{shift}} = 3/4\ N_{\text{BW}} = 30$ pixels. The resulting optical pulse burst is advanced in time by 7.5 ps, which is three times the pulse separation (2.5 ps). The relatively strong intensity peak at $t = 0$ for the experimental is, once again, attributed to the phase calibration error in modulo-2π operation. In Fig. 6(d), the spectral phase function $\Psi(\omega)$ is spectrally shifted by -200 GHz (-1.6 nm), which corresponds to 1/2 of a single period $N_{q,\text{shift}} = -1/2\ N_{\text{BW}} = -20$ pixels. The resulting optical pulse burst is delayed by 5.0 ps, which is two times the pulse separation. From the results in Fig. 6, we can see that it is possible to control the number of generated

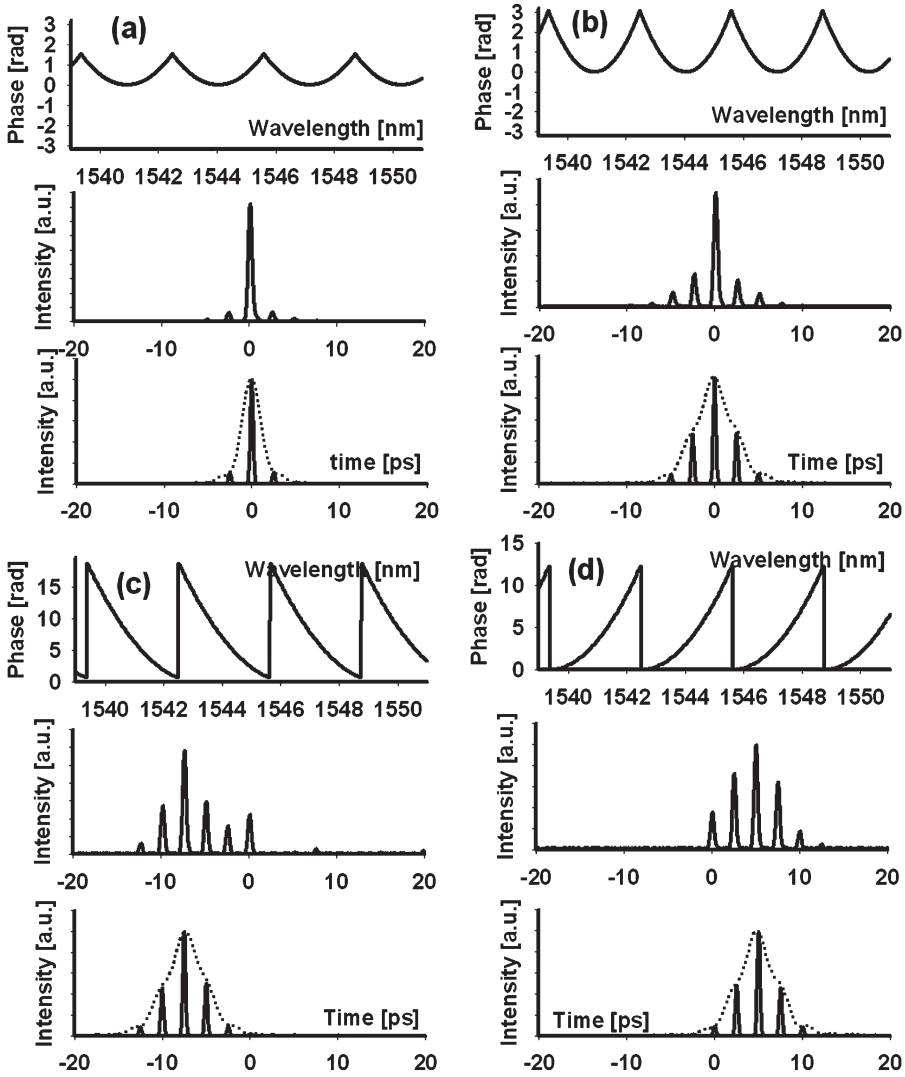

Fig. 6. Results obtained by applying periodic quadratic phase function with apparatus. Applied phase functions (top trace), resulting output intensity correlation measurements (middle trace), simulated results (bottom trace), dashed line in bottom trace is optical pulse burst envelope function: (a) Phase function varying zero to $\pi/2$. ($\Phi(n) = 0 \sim \pi/2$). (b) Phase function varying zero to π. ($\Phi(n) = 0 \sim \pi$). (c) Phase function spectrally shifted by 3/4 of single period. ($\Phi(n) = \phi_{\rm quad}(n - N_{\rm BW}/2 - 3N_{\rm BW}/4)^2$). (d) Phase function spectrally shifted by $-1/2$ of single period. ($\Phi(n) = \phi_{\rm quad}(n - N_{\rm BW}/2 + N_{\rm BW}/2)^2$).

optical pulse bursts by adjusting the quadratic phase factor $\phi_{\rm quad}$ and to shift the optical pulse burst in time by introducing a shift $(N_{q,\rm shift})$ in the quadratic spatial phase function.

Fig. 7 shows the results of applying periodic cubic phase functions. The phase functions are cubic within a single period, i.e.,

$$\Phi(n) = \phi_{\rm cubic}\left(n - \frac{N_{\rm BW}}{2} - N_{c,\rm shift}\right)^3. \qquad (10)$$

Here, the quadratic phase factor $\phi_{\rm quad}$ in (8) is set to zero and the cubic phase factor $\phi_{\rm cubic}$ is set to either -0.0005 (for negative cubic) or 0.0005 (for positive cubic) in all cases. The total bandwidth $N_{\rm BW}$ in terms of pixel numbers is equal to 40 as before. The resulting pulse bursts have temporal envelope functions (dotted line in bottom traces) that peak near $t = 0$ with asymmetric ringing on one side. This is similar to what is observed for single ultrafast pulse with cubic spectral dispersion.

Fig. 7(a)–(c) illustrates cases for a negative cubic phase function ($\phi_{\rm cubic} = -0.0005$), with no shift ($N_{c,\rm shift} = 0$), 1/4 of a period shift ($N_{c,\rm shift} =$ 1/4 $N_{\rm BW} = 10$ pixels), and 3/8 of a period shift ($N_{c,\rm shift} =$ 3/8 $N_{\rm BW} = 15$ pixels), respectively. For $N_{c,\rm shift} = 0$, the total phase variation within one period is 2π. For larger $N_{c,\rm shift}$, the total phase variation within one period increases. The resulting temporal envelope functions are all broadened toward negative time. The extent of the temporal envelope functions and the number of pulses within the burst increase with increasing $N_{c,\rm shift}$, as expected when the total phase variation increases.

Fig. 7(d)–(f) shows the results when positive cubic phase terms are applied. The settings are the same as Fig. 7(a)–(c), respectively, except a positive cubic phase factor is applied ($\phi_{\rm cubic} = 0.0005$). The results are similar to those shown in Fig. 7(a)–(c), except that the pulse bursts extend toward the positive time window. The data in Fig. 7 demonstrate that we can produce optical pulse bursts on either the positive or negative side of $t = 0$ by changing the sign of the cubic phase.

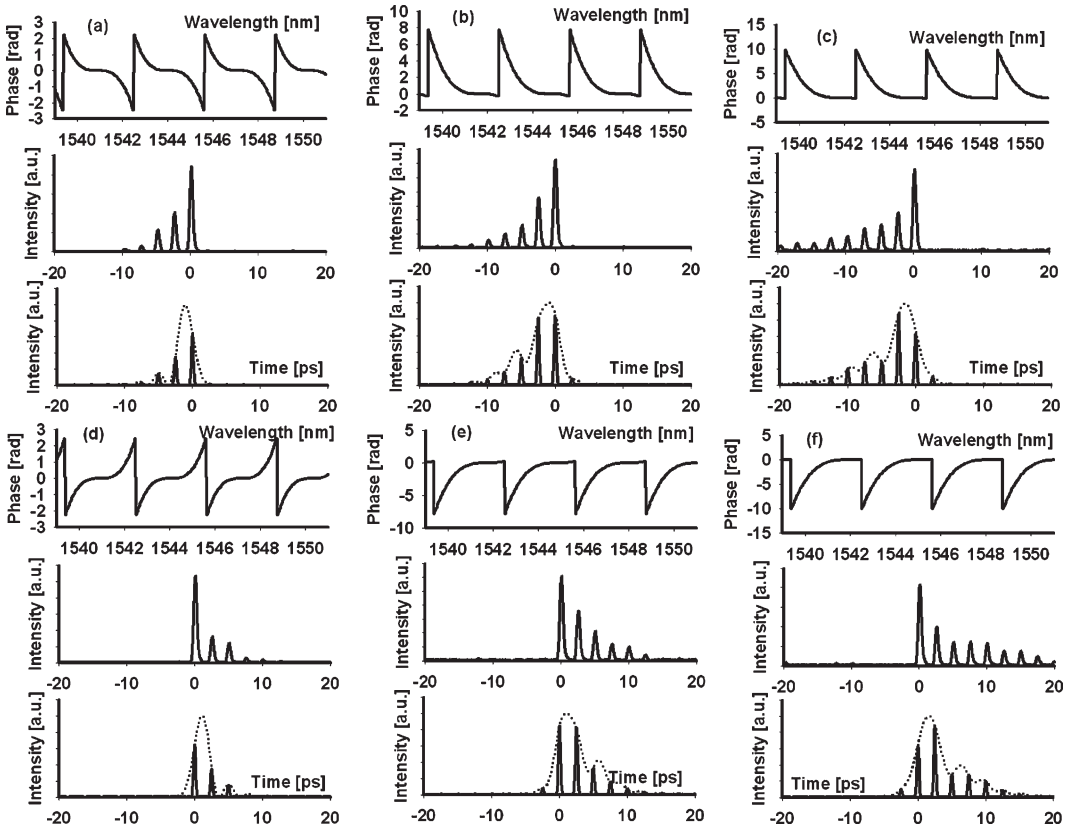

Fig. 7. Results obtained by applying periodic cubic phase function with apparatus. Applied phase functions (top trace), resulting output intensity correlation measurements (middle trace), simulated results (bottom trace): (a) Phase function varying -π to π, with negative slope ($\phi_{\rm cubic} < 0, \Phi(n) = -\pi \sim +\pi$). (b) Phase function with negative slope, spectrally shifted by 1/4 of single period ($\phi_{\rm cubic} < 0, \Phi(n) = \phi_{\rm cubic}(n - N_{\rm BW}/2 - N_{\rm BW}/4)^3$). (c) Phase function with negative slope, spectrally shifted by 3/8 of single period ($\phi_{\rm cubic} < 0$, $\Phi(n) = \phi_{\rm cubic}(n - N_{\rm BW}/2 - 3N_{\rm BW}/8)^3$). (d) Phase function varying -π to π, with positive slope ($\phi_{\rm cubic} > 0, \Phi(n) = -\pi \sim +\pi$). (e) Phase function with positive slope, spectrally shifted by 1/4 of single period (($\phi_{\rm cubic} > 0, \Phi(n) = \phi_{\rm cubic}(n - N_{\rm BW}/2 - N_{\rm BW}/4)^3$). (f) Phase function with positive slope, spectrally shifted by 3/8 of single period ($\phi_{\rm cubic} > 0, \Phi(n) = \phi_{\rm cubic}(n - N_{\rm BW}/2 - 3N_{\rm BW}/8)^3$).

Fig. 8 shows examples where binary phase patterns are applied instead of the gray level phase functions of Figs. 6 and 7. In particular, we programmed the SLM with m-sequence phase codes. For binary phase modulation, we applied zero phase ($\Phi(n) = 0$) for digit "0" and π phase ($\Phi(n) = \pi$) for digit "1". The m-sequence is a pseudorandom binary sequence often used in wireless communications and coding [14]. Due to the periodic spectral dispersion of VIPA, the single m-sequence programmed onto the SLM results in a periodic m-sequence spectral phase function. This results in a pulse burst with the number of pulses in the burst roughly equal to the length of the m-sequence code [13]. Fig. 8(a) and (b) shows the pulse bursts that result when a seven-element m-sequence (digits "0010111") and a 15-element m-sequence (digits "000100110101111") are applied, respectively. The number of pulses scales roughly with the length of the m-sequence code, as expected. Results may have application to OCDMA, where pseudorandom phase encoding/decoding is often employed [1], [2], [11].

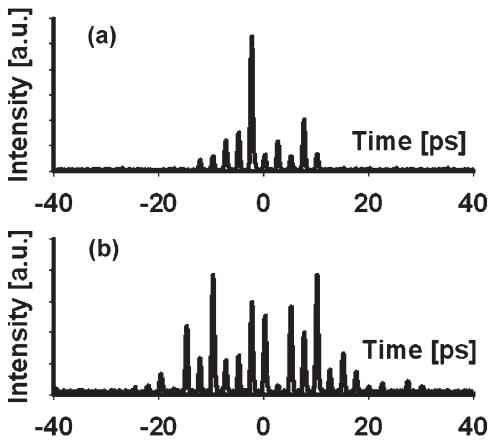

Fig. 8. Output intensity correlation measurements obtained by applying periodic m-sequence phase function with apparatus. (a) Phase function with seven-element periodic m-sequence (0010111). (b) Phase function with 15-element periodic m-sequence (000100110101111).

V. Conclusion

The authors have reported the first demonstration, to their knowledge, of programmable Fourier transform pulse shaping based on a virtuall imaged phased array (VIPA) spectral disperser. Because the experiments use ultrashort pulses with spectra broader than the free spectral range (FSR), the spatial phase function applied with the pulse shaper is replicated periodically onto the optical spectrum. The result is that the pulse shaper output is a burst of pulses, with the pulse spacing equal to the inverse of the VIPA FSR. The intensities of the individual

pulses in the burst are determined by a temporal envelope function obtained from the inverse Fourier transform of the applied spatial phase function. These effects arise specifically because of the periodic spectral dispersion provided by the VIPA and have not been observed with grating-based Fourier transform pulse shapers. The experimental data are in good agreement with the simulations. The VIPA-based Fourier transform pulse shaping scheme holds promise for programmable optical waveform synthesizers with finer spectral resolution than conventional grating-based pulse shapers. Furthermore, the work here provides evidence that previous experiments on dispersion compensation using VIPAs [7]–[9] can be understood as an example of pulse shaping.

ACKNOWLEDGMENT

The authors would like to thank Dr. D. E. Leaird for technical discussion and experimental support, and Avanex Corporation for providing the VIPA.

REFERENCES

[1] A. M. Weiner, "Femtosecond optical pulse shaping and processing," *Prog. Quantum Electron.*, vol. 19, no. 3, pp. 161–238, 1995.

[2] ——, "Femtosecond pulse shaping using spatial light modulators," *Rev. Sci. Instrum.*, vol. 71, no. 5, pp. 1929–1960, May 2000.

[3] T. Kurokawa, H. Takenouchi, and H. Tsuda, "Terabit optical signal processing based on time–space-conversion," in *Proc. Lasers and Electro-Optics Society (LEOS) 12th Annu. Meeting, IEEE*, San Francisco, CA, 1999, vol. 1, pp. 188–189.

[4] H. Tsuda, K. Okamoto, T. Ishii, K. Naganuma, Y. Inoue, H. Takenouchi, and T. Kurokawa, "Second- and third-order dispersion compensator using a high-resolution arrayed-waveguide grating," *IEEE Photon. Technol. Lett.*, vol. 11, no. 5, pp. 569–571, May 1999.

[5] M. Shirasaki, "Large angular dispersion by a virtually imaged phased array and its application to a wavelength demultiplexer," *Opt. Lett.*, vol. 21, no. 5, pp. 366–368, Mar. 1996.

[6] S. Xiao, A. M. Weiner, and C. Lin, "A dispersion law for virtually imaged phased-array spectral dispersers based on paraxial wave theory," *IEEE J. Quantum Electron.*, vol. 40, no. 4, pp. 420–426, Apr. 2004.

[7] M. Shirasaki, "Chromatic-dispersion compensator using virtually imaged phased array," *IEEE Photon. Technol. Lett.*, vol. 9, no. 12, pp. 1598–1600, Dec. 1997.

[8] ——, "Optical apparatus which uses a virtually imaged phased array to produce chromatic dispersion," U.S. Patent 20 030 021 046, Jan. 30, 2003.

[9] H. Ooi, K. Nakamura, Y. Akiyama, T. Takahara, T. Terahara, Y. Kawahata, H. Isono, and G. Ishikawa, "40-Gbps WDM transmission with virtually imaged phased array (VIPA) variable dispersion compensators," *J. Lightw. Technol.*, vol. 20, no. 12, pp. 2196–2203, Dec. 2002.

[10] S. Xiao, J. D. Mckinney, and A. M. Weiner, "Photonic microwave arbitrary waveform generation using a virtually imaged phased array (VIPA) direct space-to-time pulse shaper," *IEEE Photon. Technol. Lett.*, vol. 16, no. 8, pp. 1936–1938, Aug. 2004.

[11] S. Etemad, T. Banwell, S. Galli, J. Jackel, R. Menendez, P. Toliver, J. Young, P. Delfyett, C. Price, and T. Turpin, "Optical-CDMA incorporating phase coding of coherent frequency bins: Concept, simulation, experiment," presented at the Optical Fiber Communication Conf., Los Angeles, CA, 2004, Paper FG5.

[12] M. M. Wefers and K. A. Nelson, "Space–time profiles of shaped ultrafast optical waveforms," *IEEE J. Quantum Electron.*, vol. 32, no. 1, pp. 161–172, Jan. 1996.

[13] A. M. Weiner and D. E. Leaird, "Generation of terahertz-rate trains of femtosecond pulses by phase-only filtering," *Opt. Lett.*, vol. 15, no. 1, pp. 51–53, Jan. 1990.

[14] J. G. Proakis, *Digital Communications*, 3rd ed. New York: McGraw-Hill, 1995, pp. 724–726.

Ghang-Ho Lee (S'04) received the B.S. degree in electronics engineering from Myongji University, Seoul, Korea, in 1995, the M.S. degree in electronics engineering from Korea University, Seoul, in 1997, and is currently working toward Ph.D. degree in electrical and computer engineering at the School of Electrical and Computer Engineering, Purdue University, West Lafayette, IN.

From 1997 to 2002, he was an R&D Engineer at the Telecommunications R&D Center, Samsung Electronics Co., Ltd., Korea, performing high-speed optical transmitter/receiver design, dense wavelength division multiplexing (DWDM) transmission system benchmark test and field test with Korea Telecom, system architecture design for optical access networks and multiservice optical platform, and analysis on network strategies. His current research includes optical signal processing, optical pulse shaping, and optical fiber communications.

Mr. Lee received the Korea Government Scholarship for pursuing the Ph.D. from the Institution of Information Technology Assessment (IITA), Ministry of Information and Communication (MIC), Korea.

Andrew M. Weiner (S'84–M'84–SM'91–F'95) received the Sc.D. degree in electrical engineering from the Massachusetts Institute of Technology (MIT), Cambridge, in 1984.

From 1979 to 1984, he was a Fannie and John Hertz Foundation Graduate Fellow at MIT. Upon graduation, he joined Bellcore, Red Bank, NJ, first as member of the Technical Staff and later as the Manager of Ultrafast Optics and Optical Signal Processing Research. He moved to Purdue University, West Lafayette, IN, in 1992 and is currently the Scifres Distinguished Professor of Electrical and Computer Engineering. From 1997 to 2003, he served as the Electronics and Communications Engineering (ECE) Director of Graduate Admissions. His research focuses on ultrafast optical signal processing and high-speed optical communications. He is especially well known for pioneering the field of femtosecond pulse shaping, which enables generation of nearly arbitrary ultrafast optical waveforms according to user specification. He has published five book chapters and over 150 journal articles. He has been the author and/or coauthor of over 300 conference papers, including approximately 60 conference invited talks, and has presented over 70 additional invited seminars at university, industry, and government organizations. He is a holder of six U.S. patents.

Prof. Weiner is a Fellow of the Optical Society of America (OSA). He has served on or chaired numerous research review panels, professional society award committees, and conference program committees. From 1988 to 1989, he served as an IEEE Lasers and Electro-optics Society (LEOS) Distinguished Lecturer. He has served as Chair or Co-Chair of the Conference on Lasers and Electro-Optics, the Gordon Conference on Nonlinear Optics and Lasers, and the International Conference on Ultrafast Phenomena. He has also served as Associate Editor for the IEEE JOURNAL OF QUANTUM ELECTRONICS, IEEE PHOTONICS TECHNOLOGY LETTERS, and *Optics Letters*. He served as an Elected member of the Board of Governors of IEEE LEOS from 1997 to 1999 and as Secretary/Treasurer of IEEE LEOS from 2000 to 2002. From 2002 to 2005, he was the Vice-President (representing IEEE LEOS) of the International Commission on Optics (ICO). He has received numerous awards for his research, including the Hertz Foundation Doctoral Thesis Prize (1984), the Adolph Lomb Medal of the Optical Society of America (1990), for pioneering contributions to the field of optics made before the age of 30, the Curtis McGraw Research Award of the American Society of Engineering Education (1997), the International Commission on Optics Prize (1997), the IEEE LEOS William Streifer Scientific Achievement Award (1999), the Alexander von Humboldt Foundation Research Award for Senior U.S. Scientists (2000), and the inaugural Research Excellence Award from the Schools of Engineering at Purdue (2003).